Wear 426–427 (2019) 1781–1787

Contents lists available at ScienceDirect

Wear

journal homepage: www.elsevier.com/locate/wear

In-situ characterization of three dimensional worn surface under sliding-rolling contact

Chan Xu, Tonghai Wu*, Yanwen Huo, Hongbin Yang

Key Laboratory of Education Ministry for Modern Design and Rotor-Bearing System, Xi'an Jiaotong University, Xi'an 710049, China

ARTICLE INFO

Keywords:
In-situ characterization
Three-dimensional surface topography
Sliding-rolling contact
Surface reconstruction
Fractal dimension

ABSTRACT

Rolling bearing performance often degrades due to extra wear introduced by sliding-rolling contacts. Thus, it is vital to monitor the evolution of such wear process through investigating the worn surface. Compared with traditional two-dimensional (2-D) methods, three-dimensional (3-D) measurements of worn surfaces can provide more information. Due to the lack of in-situ 3-D measurement techniques and the scale-dependency of characterization parameters, it remains a challenge to examine the wear evolution of sliding-rolling contact using 3-D surface topography features. A characterization framework is here developed for inspecting worn surface topography variations under sliding-rolling contact, by combing 3-D surface reconstruction and computed fractal dimension. The worn surface is firstly imaged by an in-situ microscope. Next, a virtual 3-D surface is obtained from 2-D images via topography reconstruction. Then, the fractal dimension of worn surfaces is calculated to characterize the wear state with 3-D root-mean-square. A wear test is carried out on a roller-ring test rig to verify the proposed method. Results indicate that the proposed 3-D characterization performance is comparable to laser scanning confocal microscopy (LSCM) and allows rapid description of the wear process.

1. Introduction

Skidding damage of rolling bearings is a common fault in rotating machinery, which directly affects the running condition of the machine. The sliding-rolling contact may introduce extra wear that is regarded as the main cause of early failure of rolling bearings. Therefore, it is vital to monitor the evolution of such wear process [1,2]. However, previous works were emphasized on exploring the wear phenomenon by indirect measurements such as vibration [3,4], acoustic emission [5], oil-debris [6], etc. Investigation of the worn surface topography that contains abundant wear information is still a challenge. One reason is that in-situ measurements of the surface topography are often an intractable task. On the other hand, 3-D surface morphology can provide more details of wear process, when compared with 2-D images. In recent years, a number of studies have been conducted to explore 3-D surface topography changes with surface topography measurement apparatus [7–12]. Due to the miniature dimension of the object, these instruments usually require disassemble detection and are vulnerable to inaccuracies introduced.

Conventionally, surface topography is characterized by 3-D roughness parameters, such as arithmetic mean deviation, root-mean-square deviation, and maximum peak-to-valley height [13]. However, the accuracy of these parameters is highly dependent on the resolution and the scan length of the roughness-measuring instruments. Hence, these methods are scale-dependent. Alternatively, fractal theory is recently becoming a useful tool in surface texture characterization and the understanding of wear phenomena [14–17]. Existing fractal parameters, including fractal dimension (FD) and multifractal spectrum can be utilized to characterize surface topography, which are not being affected by resolution and the scan length. Its popularity in worn surface analysis is due to its ability to describe more intrinsic information of surfaces including complexity and irregularity [18,19].

The aim of this work is to characterize 3-D worn surface topography variations under sliding-rolling contact. The 3-D surface reconstruction technology and a 3-D fractal dimension computation method are adopted to recover the surface topography and to obtain surface topography features. Validation tests are conducted on a roller-ring test rig to evaluate the proposed method. The result demonstrates that the developed method is capable of in-situ measurement of 3-D worn surface topography and providing the description of wear process with 3-D surface topography features.

The rest of this paper is organized as follows. Section 2 briefly presents the 3-D surface reconstruction technology based on photometric stereo and the FD computation process. Wear tests carried out are detailed in Section 3. In Section 4, the computation of worn surfaces FD is illustrated. Performance of the proposed method is discussed in

* Corresponding author.
E-mail address: wt-h@163.com (T. Wu).

https://doi.org/10.1016/j.wear.2018.12.045
Received 4 September 2018; Received in revised form 7 December 2018; Accepted 18 December 2018
0043-1648/

the same section, followed by the main conclusion drawn in Section 5.

2. 3-D surface topography reconstruction and fractal dimension calculation

2.1. 3-D surface topography reconstruction based on the photometric stereo technology

The 3-D topography reconstruction method, photometric stereo, has been widely used in many research fields [20,21]. The principle of this method can be described as: images of the same viewpoint on the object surface under different but controllable illuminations are obtained. Based on these images and the reflection model of the object surface, the normal vector of the object surface is calculated, and then integrated to restore the object surface 3-D topography.

In this process, the Lambert reflection model is adopted [22]. Assuming that there are n light sources whose positions form a matrix (theoretically only three light sources are needed, but in practice more than three light sources are usually employed to eliminate errors), that is, $L = [L^1, L^2, \cdots L^n]^T$, where L^n represents the vector component of the nth light source. Under the action of n light sources, a set of image brightness values are obtained for the same surface point, that is, $I = [I^1, I^2, \cdots I^n]$, where I^n represents the image brightness of the surface point illuminated by the nth light source. If the normal vector of a point on the surface is $N = [n_1, n_2, n_3]^T$, the Lambert model can be expressed as a matrix:

$$N = L^{-1}I \tag{1}$$

In the following, the near point light source calibration method is used to obtain the information of the incident light, including the intensity and direction of the incident light. At the same time, according to the gray level of each pixel in the image, the reflective brightness of each point can be obtained, and the normal vector of the surface points can be calculated according to Eq. (1). The main steps are listed below.

Step 1: obtaining the photometric stereo images with the image acquisition system.

A hand-held microscope with eight circularly distributed light sources is used to obtain 2-D images of the worn surface as shown in Fig. 1. In order to obtain images of the same viewpoint on the surface, the position and intensity of the eight light sources need to be calibrated beforehand. Fig. 1(a) shows a rough and uneven worn surface. Fig. 1(b–i) show the worn surface images obtained under different illumination from the eight light sources. Each image presents different light intensity and incident light position.

Step 2: calculating the normal vector of the surface of the object.

With the images from Fig. 1, the normal vector distribution of one point on the worn surface can be calculated by using Eq. (1). By analogy, the normal direction of the photographed surface can be obtained by applying the above algorithm to all the pixels of the image.

Step 3: obtaining surface depth information by integrating the vector fields.

The obtained normal vectors are normalized, and the surface gradient domain is obtained. The depth of the surface points can be restored by integrating the normal vectors. Moreover, the surface depth is calculated by the same method as in [23]. The reconstruction 3-D surface topography is shown in Fig. 2(a).

In order to verify the accuracy, a comparison with the 3-D surface imaged by LSCM was carried out, see Fig. 2(b). The resolution of the reconstructed image is 600 × 600, and the resolution of the LSCM image is 1024 × 1024. Because it remains difficulty to find the exact location corresponding to the reconstructed surface, as depicted in Fig. 2, feature points cannot be aligned precisely. Despite the different sampling lengths and resolutions, the result of the proposed reconstruction method qualitatively matches the results from the LSCM.

According to the height data from reconstructed surfaces and surfaces captured by the LSCM, two basic 3-D roughness parameters: the arithmetic mean deviation S_a and the root-mean-square deviation S_q, are calculated and displayed in Table 1. Contrast results show that the accuracy of reconstructed results is over 80%.

Although the reconstructed surface morphology is highly consistent with the LSCM image, the accuracy of reconstructed surface is still affected by many factors: (i) The effect of resolution. The higher the image resolution is, the richer details of the image are, and the longer the calculation time is. Here, the original image resolution is 600 × 600, corresponding to 1.33 µm per pixel. For the worn surface, this accuracy is sufficient. (ii) The clarity of photometric stereo image. It is necessary to clean the worn surface and focus the camera to acquire a clear image. The light intensity of the environment should be as low as possible. Otherwise, the accuracy of reconstruction results will be affected. (iii) Verification of reconstructed results. Fig. 2 shows that LSCM cannot be exactly corresponded to the reconstructed position. This is because the focusing position can only be determined by salient features of the reconstructed surface when using LSCM to acquire the image. This remains a problem that needs to be solved in the future.

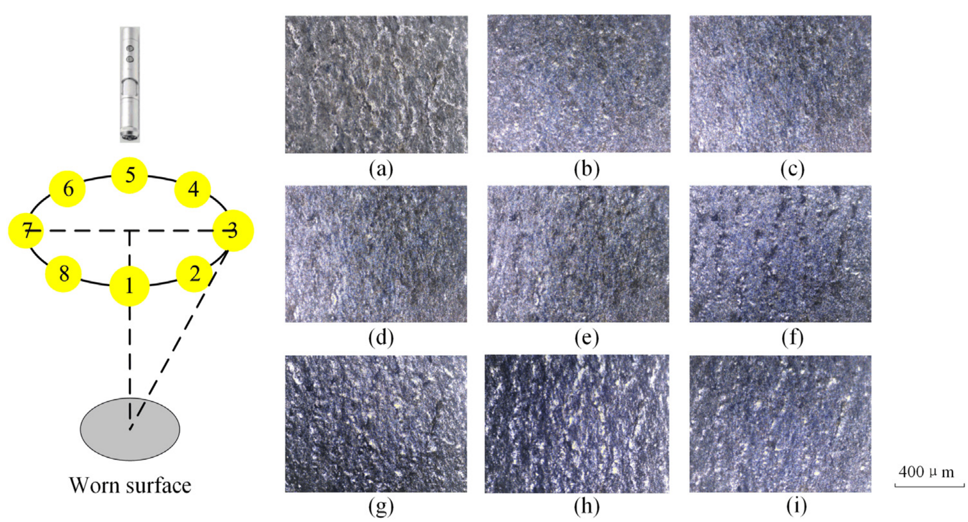

Fig. 1. 3-D surface topography reconstruction schematic diagram, (a) image with all eight lights on, (b–i) images sequentially obtained under the different light from 1 to 8.

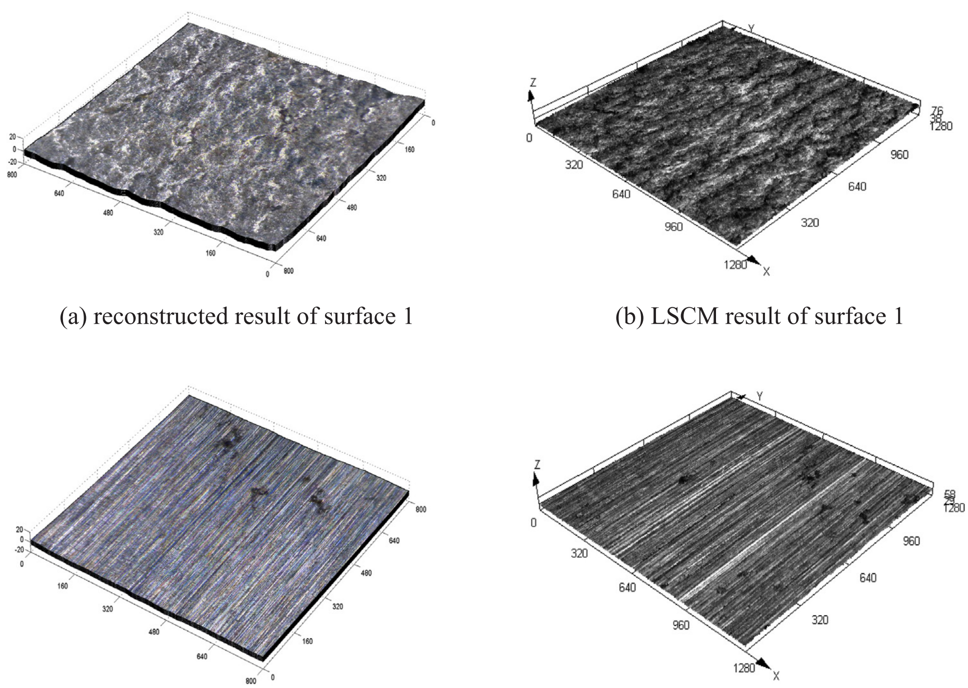

(a) reconstructed result of surface 1 (b) LSCM result of surface 1

(c) reconstructed result of surface 2 (d) reconstructed result of surface 2

Fig. 2. Results of 3-D surfaces with different methods, (a, c) reconstructed image, (b, d) LSCM image.

Table 1
Accuracy verification results.

Surface	Roughness	Reconstruction	LSCM	Accuracy
1	S_a	1.702	2.103	89.1%
	S_q	1.910	2.538	82.9%
2	S_a	1.340	1.845	80.6%
	S_q	1.662	2.178	84.7%

2.2. Fractal dimension calculation based on the 3D-RMS method

Fractal geometry characterized by scale-independent and self-affinity, can be used to describe the topography of worn surfaces [24]. Various computation methods of FD have been proposed over recent years, such as differential box-counting [25], triangular prism area surface [26] and variation method [27]. In comparison, the expressions of these methods can be unified and expressed as:

$$D = -\lim_{\tau \to 0} \frac{\log(M)}{\log(\tau)} \tag{2}$$

where M is the measure of the calculation method, τ is the corresponding scale, D is the fractal dimension. Therefore, if the measure and the scale can be selected properly and the power exponent relationship in Eq. (2), can be established, then the corresponding fractal dimension can be obtained.

However, all the current methods cannot provide high enough accuracy. Therefore, a new method, three-dimensional root-mean-square (3D-RMS), is applied to conquer the problem [19]. The basis of 3D-RMS method is the root-mean-square value of the surface heights. Root-mean-square is a statistical parameter and is calculated by using all the height data on the surface, which makes the 3D-RMS method more accurate.

According to [19], the root-mean-square $V(r)$ follows the power law computed by

$$\log V(r) = (3 - D)\log r \tag{3}$$

where $V(r)$ is the measure of the method, r is the corresponding scale, D is the FD. As can be seen from Eq. (3), the double logarithmic graph of $\log V(r)$ versus $\log(r)$ can be used to estimate the FD

$$D = \lim_{r \to 0}\left[3 - \frac{\log V(r)}{\log(r)}\right] \tag{4}$$

The detailed steps of 3D-RMS method are shown as follows.

(i) The surface topography data are presented in a $N \times N$ matrix. $z(x, y)$ is the surface height value at position (x, y). The projection area of the surface on the XOY plane is divided into $K \times K$ non-overlapping square units, where $K = \min\{floor[N/r]\}$, $floor[\bullet]$ denotes rounding to the next smaller integer, r denotes the side length of a square neighborhood. Let $C(k, l)$ denotes the square in the kth row and lth column, $k, l = \{1, 2, \cdots K\}$. Fig. 3 shows the partitioning of the squares.

(ii) The root-mean-square of all height values in the square unit $C(k, l)$ can be expressed as:

$$V(r) = \sqrt{E\{\,[z(x, y) - E\{z(x, y)\}]^2\}}, \qquad (x, y) \in C(k, l) \tag{5}$$

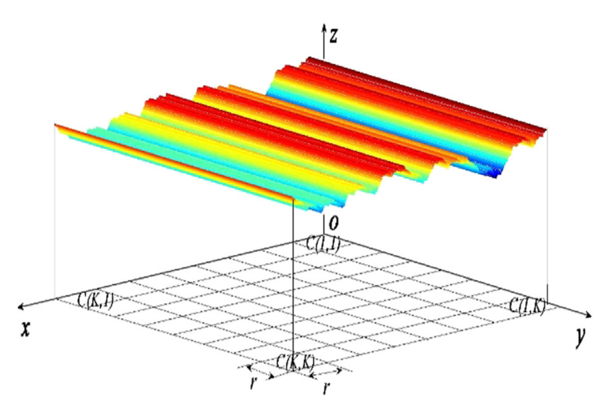

Fig. 3. An illustration for the partition method of squares.

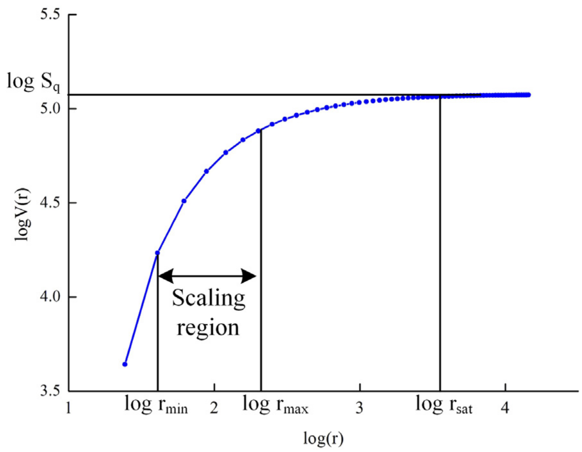

Fig. 4. Schematic of the scaling region.

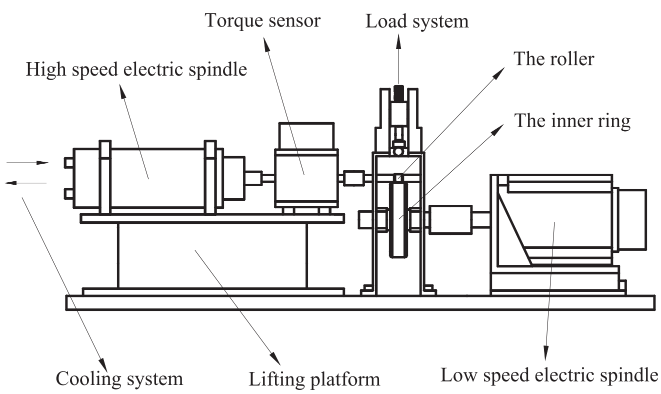

Fig. 5. Schematic diagram of the test rig.

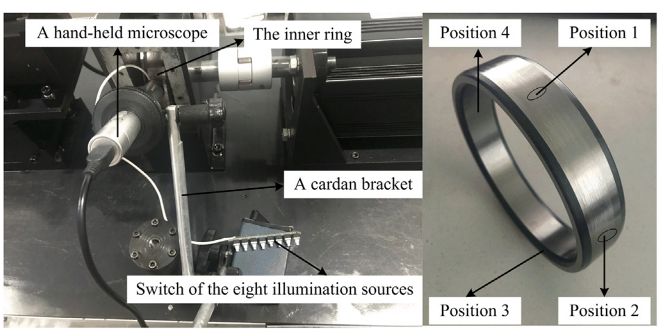

Fig. 6. In-situ measurement apparatus.

(iii) Repeat step (ii) for each square. According to Eq. (3), the following can be obtained from the fact that the root-mean-square $V(r)$ for the whole surface and the side length are related in terms of an exponential function:

$$V(r) = E\{v(r)\} \sim r^{(3-D)} \tag{6}$$

(iv) Change the side length r and repeat steps (i)–(iii), the corresponding root-mean-square $V(r)$ can be obtained iteratively. According to Eq. (4), the FD of surface can be estimated by the slope α in the double logarithmic graph, namely, $D = 3 - \alpha$.

The scale-invariant FD provides geometric structure at certain regions called scaling region. When calculating the FD, the scaling region can be simply considered as a straight-line portion of the entire double logarithm curve. Fig. 4 shows the log $V(r)$ versus log(r) plot obtained from 3D-RMS, where $r_{\min}$ and $r_{\max}$ are the lower limit and upper limit of the scale region respectively. Then, points (log(r), log $V(r)$) between $r_{\min}$ and $r_{\max}$ in the double logarithm graph are calculated by least square fit. The slope of the fitted line is obtained, and then the FD of surface can be calculated.

The measured $V(r)$ of 3D-RMS has close relation with the root-mean-square deviation S_q. On one hand, Fig. 4 shows that log $V(r)$ increases and becomes stabile with the increasing log(r). The corresponding scale of the first stable point is r_{sat}. Calculations prove that the saturated measure V_{sat} is equal to the surface root-mean-square deviation S_q. On the other hand, surface root-mean-square deviation S_q will be underestimated when the side length of measured area is less than r_{sat}. Because in this case larger area contains more characteristics such as peaks and valleys, and gives rise to surface roughness. Thus, it is inaccurate to calculate S_q for a smaller scale.

Table 2
Operation conditions.

Lubricating oil	Slip ratio	Rotational speed of the roller	Radial load
Base oil	0.4	7500 rpm	2000 N

3. Experiments and in-situ measurement of worn surface

3.1. Experiment apparatus and operating conditions

The roller-ring test rig was constructed using a roller of 10 mm diameter and an inner ring of 108 mm diameter from a NU209EM bearing, see Fig. 5. In the experiments, the roller and the inner ring were driven by two independent electric spindles. Thus, the rolling-sliding motion can be accomplished by varying the slip ratio. The roller speed was ranged from 0 rpm to 10,000 rpm, and the inner ring speed was ranged from 0 rpm to 4000 rpm. Load was applied vertically on the roller via a lever system with a load sensor providing the feedback. Lubricating oil was injected by a peristaltic pump into the sliding-rolling contact region, then returned to the tank for cooling. The temperature of the lubricating oil can be controlled by a heating rod in the oil tank.

The test rig allows "in-situ" observation of the inner ring surface during interrupted tests, thus avoids dismounting the specimens, to avoid a major cause of inaccuracy. The in-situ inspection device consists of a hand-held microscope with 30X magnification and a cardan bracket as shown in Fig. 6. The microscope can be extended into the test rig to observe the surface topography, and the cardan bracket was used to adjust the focal length and ensure location precision.

Accelerated experiments were carried out under the operation conditions shown in Table 2. Four markers were drawn on the inner ring. The tests were interrupted every hour and the four positions are imaged at each interruption. The total test duration is 10 h. In order to obtain a trend of the inner ring in different wear condition, the test was carried out with no lubricant for dry friction during the 4th to 10th hours.

3.2. Experiment results

With the reconstruction method described in Section 2.1, the 2-D photometric stereo images are used to reconstruct the 3-D worn surface topography. Reconstructed results of typical worn surface topography in different wear stages are shown in Fig. 7, including no wear, normal wear and severe wear. In the 3-D graphs, the coordinate units of x, y and z axes are all in microns. It can be seen in Fig. 7(a) that the surface is damage free while a lot of scratches appear on the worn surface as shown in Fig. 7(b). It is found in Fig. 7(c) that large changes have taken place on the surface due to poor lubrication. According to the change of

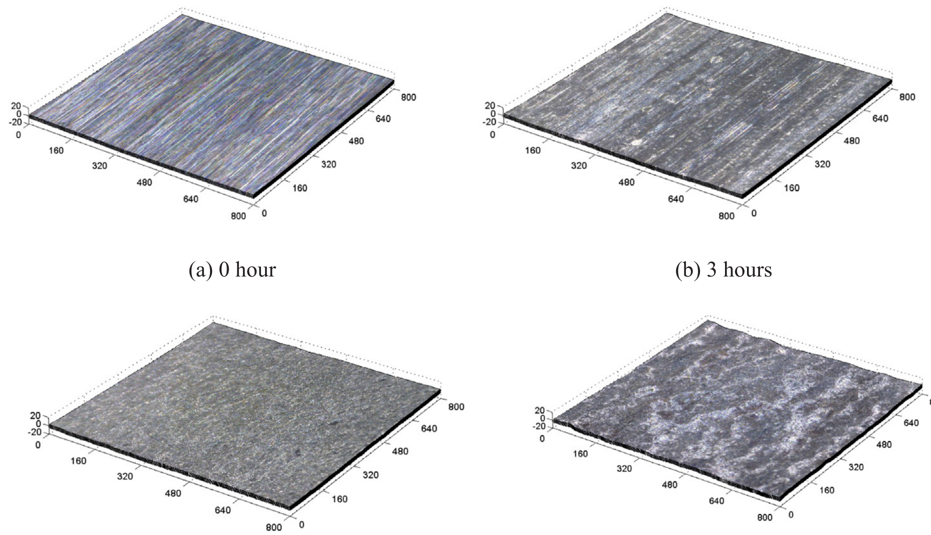

(a) 0 hour (b) 3 hours

(c) 5 hours (d) 10 hours

Fig. 7. Surface degradation process of the inner ring, (a) 3-D image of surface morphology at 0 h, (b) 3 h, (c) 5 h, (d) 10 h.

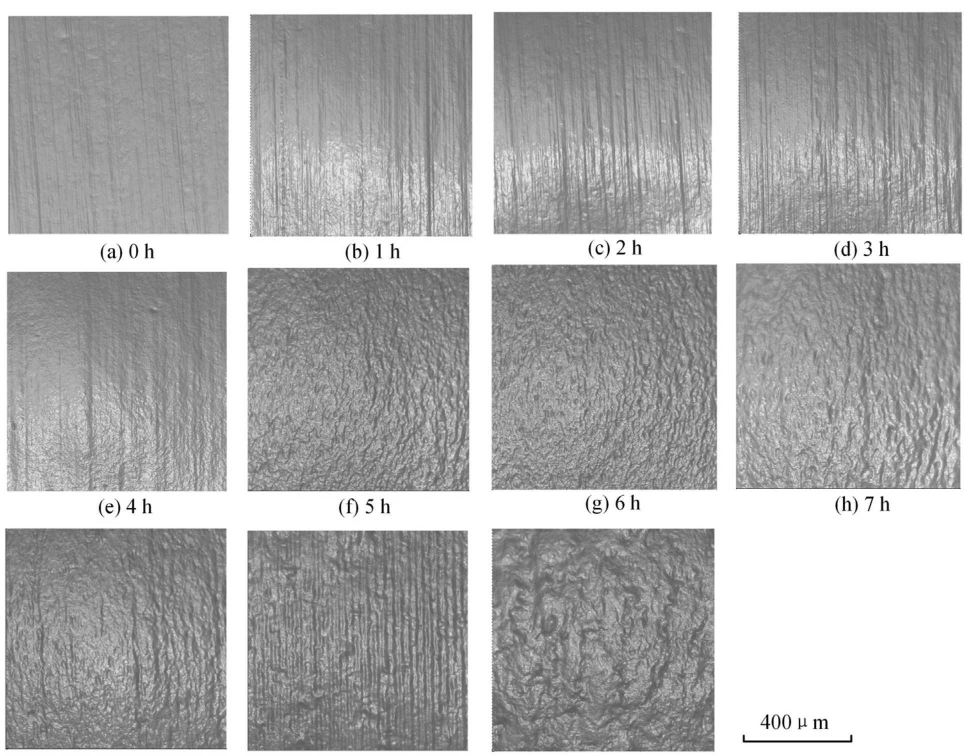

(a) 0 h (b) 1 h (c) 2 h (d) 3 h

(e) 4 h (f) 5 h (g) 6 h (h) 7 h

(i) 8 h (j) 9 h (k) 10 h

Fig. 8. The reconstructed surfaces of position 1, (a) 3-D image of surface morphology at 0 h, (b) 1 h, (c) 2 h, (d) 3 h, (e) 4 h, (f) 5 h, (g) 6 h, (h) 7 h, (i) 8 h, (j) 9 h, (k) 10 h.

surface morphology and color, it can be preliminarily judged that adhesive wear may occur at this time. Fig. 7(d) indicates that spalling occurred at 10th hour.

In order to show the slight change of the surface morphology during the whole wear process, the gray image of the surface morphology is used to analyze the wear process, as shown in Fig. 8. Fig. 8(a) indicates that fine finishing makes the original surface of the inner ring a relatively uniform roughness. Fig. 8(b–d) show that the surface is becoming roughened after 3 h of normal wear under good lubrication condition, and surface scratches are getting more and deeper. After stopping the oil circulation, scratches become shallow and the surface topography changes slightly, see Fig. 8(e). A large number of pits can be observed on the surface as shown in Fig. 8(f–h), which are caused by adhesive wear. Fig. 8(i–j) shows that severe abrasive wear has occurred on the surface, caused by a large number of abrasive particles produced in the adhesive wear process. As the temperature of the contact area increases, the wear is intensified, and large spalling occurs on the surface, see Fig. 8(k). According to the surface depth information, 3-D features can be extracted using 3D-RMS for quantitative analysis of wear process.

Table 3
FD and S_q of worn surfaces during the wear process.

Time	Position 1		Position 2		Position 3		Position 4	
	FD	S_q	FD	S_q	FD	S_q	FD	S_q
0 h	2.6882	0.4658	2.6880	0.6366	2.6882	0.5120	2.6883	0.5506
1 h	2.6880	0.5534	2.6876	0.6053	2.6876	0.6786	2.6876	0.5675
2 h	2.6877	0.5919	2.6876	0.5915	2.6877	0.5835	2.6875	0.6047
3 h	2.6874	0.5832	2.6874	0.6310	2.6874	0.6019	2.6874	0.5971
4 h	2.6875	0.6381	2.6875	0.6098	2.6876	0.6051	2.6875	0.5974
5 h	2.6874	0.6784	2.6874	0.6746	2.6874	0.6429	2.6874	0.6752
6 h	2.6875	0.6850	2.6874	0.6493	2.6875	0.6285	2.6874	0.6321
7 h	2.6874	0.6658	2.6874	0.8294	2.6874	0.7750	2.6874	0.7702
8 h	2.6874	0.6874	2.6875	0.6285	2.6876	0.5576	2.6875	0.6695
9 h	2.6877	0.6771	2.6877	0.6722	2.6876	0.6213	2.6876	0.6405
10 h	2.6879	0.5733	2.6878	0.6334	2.6877	0.6518	2.6877	0.5058

4. Characterization of 3-D worn surface using FD

The FD of the friction pair surface can reflect the complexity, roughness and self-similarity of the 3-D worn surface topography. The larger the FD is, the more complex the 3-D surface topography is. Furthermore, the more detailed structure is, the smaller the roughness is, and the stronger the self-similarity between the whole and local topography is. The FD is calculated based on the 3D-RMS method described in Section 2.2. As a typical roughness parameter, the surface root-mean-square deviation S_q is also computed for comparison, as shown in Table 3 and Fig. 9.

As can be seen from Table 3, the value of FD actually changes very little. This is because the inner ring used in the experiment comes from the real rolling bearing, and the wear duration of the experiment is much shorter than the lifespan of the rolling bearing in practice. Therefore, the change of the wear surface is very small, and the calculated FD is also small. However, according to the repetitive experimental results, FD follows the same fluctuation behavior in the four positions. It decreases dramatically at first, stabilizes at a low value, and increases slowly at the end. By contrast, S_q increases rapidly at first, fluctuates around a high value then, and decreases slowly at the end.

On the other hand, statistical parameters can only indicate that the wear surface has changed but cannot explain the wear state of the surface. By combining the 3-D surface morphology in different wear stage in Figs. 7 and 8, the decrease, stability and increase of FD can quantitatively reflect the topography changes of the worn surface during the wear process under sliding-rolling contact.

During the time from 0 h to 3 h, the inner ring surface is under normal wear and the detailed structures of the original surface are destroyed, making roughness to increase and the FD decreases. During the period from 3 h to 5 h, due to oil-free lubrication, adhesion wear occurs. Scratches become shallow and a lot of adhesive particles are produced on the surface, causing increased roughness and small fluctuations in FD. During the period from 5 h to 9 h, adhesive particles are smoothened, and severe abrasive wear occurs. A large number of scratches are produced on the surface, the number of detailed structures are increasing, causing the roughness to increase, the FD remains at a stable value and then increases. During the period from 9 h to 10 h, wear is intensified with the occurrence of spalling fatigue. A large amount of detailed structures is produced, the self-similarity between the whole and local topography is becoming stronger, and the FD increases slowly.

Therefore, FD can reflect the essential properties of surface topography regardless of scale, while the roughness parameter is only a numerical representation of the height of the surface profile. Different measuring instruments will show different roughness values and the roughness parameters cannot be calculated accurately for a smaller scale. Thus, for limited surface data, it is more reliable to characterize the surface topography by FD than roughness parameters.

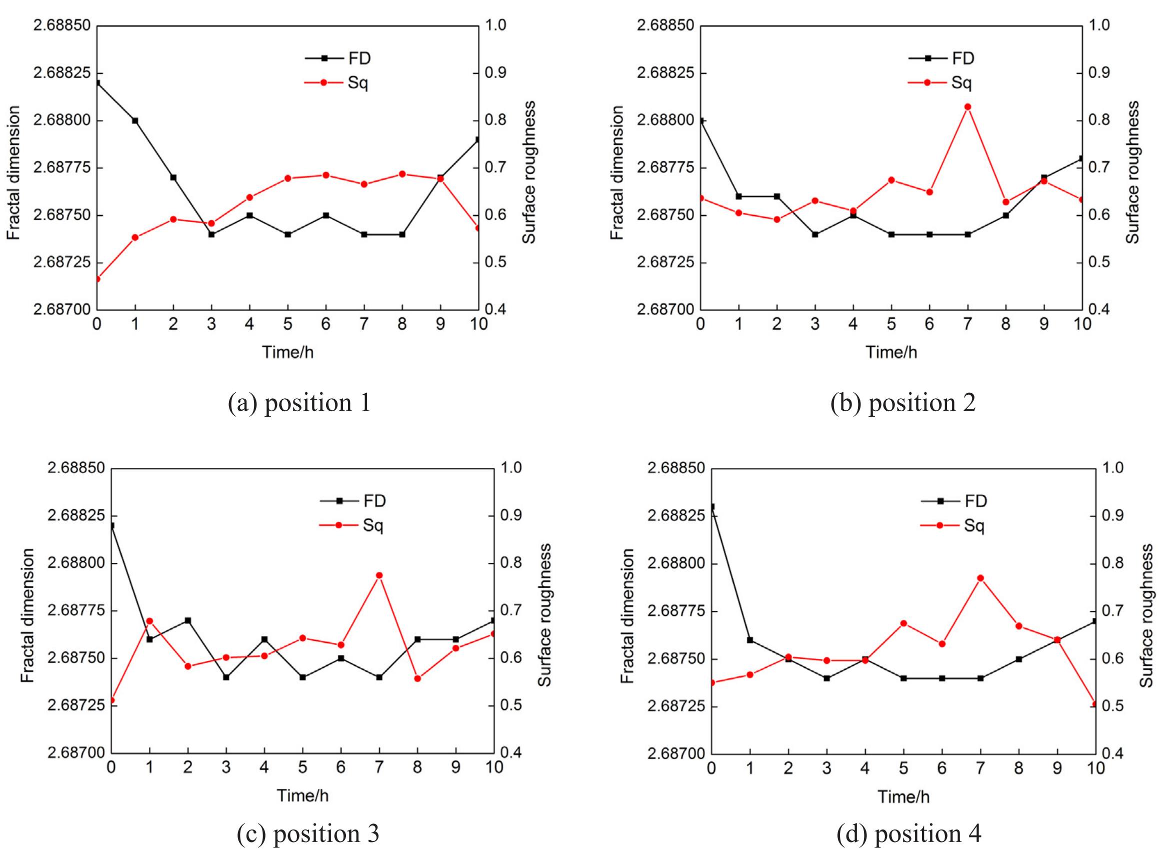

Fig. 9. Variation of FD and S_q during the wear process, (a) position 1, (b) position 2, (c) position 3, (d) position 4.

5. Conclusions

In this paper, a framework for in-situ characterization of worn surface under sliding-rolling contact is presented. An in-situ measurement method and 3-D surface reconstruction are adopted to obtain the 3-D surface morphology of the inner ring. Then a 3-D fractal dimension computation method is used to extract 3-D surface morphology features and the wear evolution of sliding-rolling contact can be characterized by the extracted fractal features. The main conclusions can be summered as follows.

(1) The 3-D surface reconstruction technique provides a new way for in-situ measurement of 3-D worn surface without disassemble detection. The reconstructed surface has high consistency with the surface captured by LSCM. The reconstructed surface topography can be used for qualitative analysis, and the height data can be used for quantitative analysis of 3-D worn surface.
(2) The fractal dimension can be used for characterization of 3-D worn surfaces under sliding-rolling contact. It decreases rapidly at first, fluctuates around a lower value then, and increases slowly in the end: reflecting the topography changes of the worn surface in different periods of the wear process.
(3) The fractal dimension can reflect the essential properties of surface morphology regardless of scale. For limited surface data, it is more reliable to characterize the wear evolution by using fractal dimension than roughness parameters.

Acknowledgements

This work is funded by the National Science Foundation of China, China (Grant No. 51675403), the NSFC-Zhejiang Joint Fund for the Integration of Industrialization and Informatization, China (Grant No. U1709215), and the International Collaborative Plan of Shaanxi Province, China (Grant No. 2017kw-034). The author also gratefully acknowledges the support of K. C. Wang Education Foundation, China.

References

[1] I. El-Thalji, E. Jantunen, A summary of fault modelling and predictive health monitoring of rolling element bearings, Mech. Syst. Signal Process. 60–61 (2015) 252–272.
[2] I. El-Thalji, E. Jantunen, A descriptive model of wear evolution in rolling bearings, Eng. Fail. Anal. 45 (2014) 204–224.
[3] T.J. Harvey, R.J.K. Wood, H.E.G. Powrie, Electrostatic wear monitoring of rolling element bearings, Wear 263 (2007) 1492–1501.
[4] N. Sawalhi, R.B. Randall, Vibration response of spalled rolling element bearings: observations, simulations and signal processing techniques to track the spall size, Mech. Syst. Signal Process. 25 (2011) 846–870.
[5] A.M. Al-Ghamd, D. Mba, A comparative experimental study on the use of acoustic emission and vibration analysis for bearing defect identification and estimation of defect size, Mech. Syst. Signal Process. 20 (2006) 1537–1571.
[6] Z. Peng, N. Kessissoglou, An integrated approach to fault diagnosis of machinery using wear debris and vibration analysis, Wear 255 (2003) 1221–1232.
[7] H. Zhu, X. Zuo, Y.K. Zhou, Recurrence evolvement of brass surface profile in lubricated wear process, Wear 352–353 (2006) 9–17.
[8] C.Q. Yuan, Z. Peng, X.P. Yan, X.C. Zhou, Surface roughness evolutions in sliding wear process, Wear 265 (2008) 341–348.
[9] U. Olofsson, S. Björklund, 3-D surface analysis of worn spherical roller thrust bearings, Int. J. Mach. Tools Manuf. 38 (1998) 485–493.
[10] F. Cabanettes, B.G. Rosén, Topography changes observation during running-in of rolling contacts, Wear 315 (2014) 78–86.
[11] L. Berthe, P. Sainsot, A.A. Lubrecht, M.C. Baietto, Plastic deformation of rough rolling contact: an experimental and numerical investigation, Wear 312 (2014) 51–57.
[12] N.F.M. Yusof, Z.M. Ripin, A technique to measure surface asperities plastic deformation and wear in rolling contact, Wear 368–369 (2016) 496–504.
[13] N.F.M. Yusof, Z.M. Ripin, Analysis of surface parameters and vibration of roller bearing, Tribology Trans. 57 (2014) 715–729.
[14] T.R. Thomas, B.G. Rosén, N. Amini, Fractal characterization of the anisotropy of rough surfaces, Wear 232 (1999) 41–50.
[15] A.L. Wang, C.X. Yang, X.G. Yuan, Evaluation of the wavelet transform method for machined surface topography 2: fractal characteristic analysis, Tribol. Int. 36 (2003) 527–535.
[16] M.C. Kang, J.S. Kim, K.H. Kim, Fractal dimension analysis of machined surface depending on coated tool wear, Surf. Coat. Technol. 193 (2005) 259–265.
[17] Z. Jiang, H. Wang, B. Fei, Research into the application of fractal geometry in characterising machined surfaces, Int. J. Mach. Tools Manuf. 41 (2001) 2179–2185.
[18] P. Podsiadlo, G.W. Stachowiak, Fractal-wavelet based classification of tribological surfaces, Wear 254 (2003) 1189–1198.
[19] X. Zuo, Z. Hua, Y.K. Zhou, Y. Li, A new method for calculating the fractal dimension of surface topography, Fractals 23 (2015) 1550022.
[20] S. Herbort, C. Wöhler, An introduction to image-based 3D surface reconstruction and a survey of photometric stereo methods, 3D Res. 2 (2011) 1–17.
[21] R. Mecca, A. Wetzler, A.M. Bruckstein, R. Kimmel, Near field photometric stereo with point light sources, Siam J. Imaging Sci. 7 (2014) 2732–2770.
[22] W.Y Xie, Z. Song, X.T. Zhang, A novel photometric method for real-time 3D reconstruction of fingerprint, in: Proceedings of International Symposium on Visual Computing, 2011, pp. 31–40.
[23] A.K. Agrawal, R. Raskar, R. Chellappa, What is the range of surface reconstructions from a gradient field? Lect. Notes Comput. Sci. 1 (2006) 578–591.
[24] S. Spasić, On 2D generalization of Higuchi's fractal dimension, Chaos Solitons Fractals 69 (2014) 179–187.
[25] N. Sarkar, B.B. Chaudhuri, An efficient differential box-counting approach to compute fractal dimension of image, IEEE Trans. Syst. Man Cybern. 24 (1994) 115–120.
[26] K.C. Clarke, Computation of the fractal dimension of topographic surfaces using the triangular prism surface area method, Comput. Geosci. 12 (1986) 713–722.
[27] B. Dubuc, S.W. Zucker, C. Tricot, J.F. Quiniou, Evaluating the fractal dimension of surfaces, Proc. R. Soc. Lond. 425 (1989) 113–127.